Direct RFOC Strategies Aimed to Symmetrical Two-Phase IM Drives: Comparison Between B4- and B6-Inverters in the Stator

Ameni Ouarda, Bassem El Badsi, and Ahmed Masmoudi, *Senior Member, IEEE*

***Abstract*—This paper deals with an investigation of the steady-state and transient performance of the direct rotor flux-oriented control (RFOC) strategies implemented in symmetrical two-phase induction motors (2PIMs). Such an investigation is structured within a comparison study considering: 1) the case of a two-leg voltage source inverter (B4-inverter), and 2) the case of a three-leg voltage source inverter (B6-inverter), in the stator of the 2PIM. Following a presentation of both drives, the principle of the RFOC is briefly recalled. Then, a special attention is paid to the implementation of the direct RFOC on current-regulated B4- and B6-inverters. The control of the power switches is achieved by two two-level hysteresis regulators in the B4-inverter rather than three in the B6-inverter. Initiated by a simulation-based analysis of the selected steady-state features of both 2PIM drives under direct RFOC strategies, the comparison study is then extended to a deep experimental investigation of the steady-state operation with emphasis on the dc-link capacitor voltages, the stator line-to-line and phase voltages, stator phase currents, the rotor flux, and the electromagnetic torque. The established results reveal three major limitations of the B4-inverter fed 2PIM drive, such as: 1) unbalanced dc-link capacitor voltages at low speeds; 2) a reduced speed range due to the low level of the phase voltages; and 3) an injection of harmonics due to the *d–q* transformation. While the B6-inverter exhibits balanced dc-link capacitor voltages in the total constant torque region with higher ripple of the stator phase currents and of the electromagnetic torque, the experiment-based comparison is achieved by an investigation of the dynamic behaviors of both drives under step- and ramp-shaped reversals of the reference speed. It highlights the poor dynamic behavior of the B4-inverter fed 2PIM drive under both shapes of speed reversal.**

***Index Terms*—B4-inverter, B6-inverter, comparison study, experimental investigation, rotor flux-oriented control (RFOC), simulation, steady-state operation, symmetrical two-phase induction motor (2PIM), transient behavior.**

I. Introduction

FOLLOWING the alarming increase of the rare-earth permanent magnet (PM) cost that greatly disturbed the automotive industry in the middle of 2011, intensive R&D projects have developed in an attempt to substitute brushless motor-based embedded actuators by PM-less ones. Of particular interest is the squirrel cage induction motor (IM) in so far as its manufacturing has reached a high level of maturity.

Accounting for the limited power range of the automotive actuators (apart the propellers integrated in the electric and hybrid propulsion systems), and for the sake of an improvement of the compactness, the conventional three-phase induction motor (3PIM) could be substituted by a symmetrical two-phase one, yielding the so-called two-phase induction motor (2PIM). Basically, this latter produces a pure circular rotating field if the two stator phases are fed by sinusoidal currents sharing the same amplitude and angular frequency, and shifted by 90°.

Unlike 3PIMs integrated in variable speed drives, symmetrical 2PIMs could be fed by different inverter topologies, including [1]–[3] the following.

1) The B4-inverter, which is made up of two legs. The motor phases are series connected with the terminal of each linked to a leg of the B4-inverter while the neutral point linked to the middle point of the dc bus voltage.
2) The B6-inverter, which is made up of three legs. The motor phases are series connected with the terminal of each as well as the neutral point linked to a leg of the B6-inverter.
3) The B8-inverter, which is made up of four legs. The motor phases are totally disconnected with the terminals of each one linked to two legs of the B8-inverter.

In large-scale production industries such as the automotive and home appliance ones, the cost effectiveness is a key issue. Within this statement, reduced-structure inverters offer crucial cost benefit. This makes the B4- and B6-inverters viable candidates to feed 2PIM-based actuators, with a superiority in favor of the B4 one.

This said, it is commonly believed that the cost effectiveness represents a tradeoff with the drive performance. Indeed, there is a required level of performance to be fulfilled by 2PIM drives even in low-cost applications. Within this framework, several works have been reported in the literature dealing with the improvement of the steady-state features and transient behavior of 2PIM drives with emphasis on the proposal of dedicated pulse width modulation (PWM) techniques under open-loop operation on one hand, and the synthesis of closed-loop control strategies on the other hand.

Vieira et al. proposed, in [4], a PWM approach for B6-inverter fed 2PIM drives, enabling the generation of symmetri-

Manuscript received May 1, 2017; revised October 11, 2017 and November 25, 2017; accepted January 5, 2018. Date of publication January 23, 2018; date of current version August 7, 2018. Recommended for publication by Associate Editor J. Zhang. *(Corresponding author: Ahmed Masmoudi.)*

The authors are with the Laboratory of Renewable Energies and Electric Vehicles, National Engineering School of Sfax, University of Sfax, Sfax 3038, Tunisia (e-mail: ameniouarda@gmail.com; bassemelbedsi@yahoo.fr; a.masmoudi@enis.rnu.tn).

Color versions of one or more of the figures in this paper are available online at http://ieeexplore.ieee.org.

Digital Object Identifier 10.1109/TPEL.2018.2795644

cal and asymmetrical stator voltages. It has been shown that the amplitudes of line-to-line voltages can vary from zero to 0.707 per unit of dc-link voltage for symmetrical voltages. The performance of the proposed PWM approach has been demonstrated by simulation and validated by experiments.

In [5], *Kumsuwan et al.* proposed a carrier-based unbalanced PWM strategy for B8-inverter fed asymmetrical 2PIM drives. The proposed strategy is based on the unipolar modulation technique with open-loop V/f control. It enables the generation of two-phase output voltages with independently adjustable magnitudes and quadrature phase angle.

Different discontinuous space vector (SV)-PWM techniques for a B6-inverter fed symmetrical two-phase loads have been proposed in [6]. A special attention has been paid to the reduction of the inverter switching loss and the output current ripple. The investigation covered both balanced and unbalanced output phase voltages at high modulation index considering a load power factor angle of 30° lagging. The performance of the proposed techniques have been demonstrated by simulation and experiments along with a comparison with those exhibited by a continuous SV-PWM technique.

Concerning the closed-loop control strategies, *Jemli et al.* proposed a sensorless indirect stator flux-oriented control devoted to 2PIM drives [7]. The speed estimation is based on the measurement of the stator main and auxiliary phase currents. The performance of the proposed strategy has been demonstrated by simulation and validated by experiments. It has been found that, at very low speeds including standstill, these performance are sensitive to the accuracy of the stator and rotor resistances. In order to overcome this problem, the authors proposed an online resistance estimation as an outlook of their work.

In [8], *Guerreiro et al.* introduced an approach to control the speed of asymmetrical and symmetrical 2PIMs. It consists in a step commutation of the voltage phase so that the resulting voltage phasor turns to be diametrically opposed to the initial, yielding the so-called "diametrical inversion" (DI) technique. The DI has been allied to a sliding mode technique to implement a speed controller for 2PIM drives.

It has been shown that the DI technique offers a high dynamic of the torque, and that the sliding mode guarantees a high robustness against external torque disturbances.

In [9], *Kascak et al.* treated the SV-PWM-based indirect rotor flux-oriented control (RFOC) of 2PIM drives considering both cases of B6-inverter and matrix half-bridge converter in the motor stator. A special attention has been paid to the switching sequence for the SV-PWM technique in order to minimize the output current ripple. An indirect RFOC scheme has been proposed and implemented. Simulation and experimental results confirmed the performance of the proposed strategy.

In [10], *Jang* focused on the problems allied to the implementation of indirect RFOC strategies on asymmetrical 2PIM drives. These problems are encountered starting from the motor parameters identification. These could be overcome considering symmetrical 2PIMs for which an indirect RFOC strategy has been implemented. The proposed strategy has been inspired from the indirect vector control strategy proposed so far for three-phase ac machines. The drive performance have been verified by simulations and experiments.

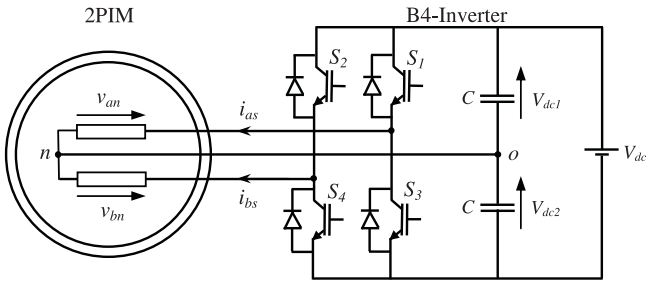

Fig. 1. B4-inverter fed 2PIM drive connections.

In [11], *Nied et al.* considered the implementation of an indirect RFOC strategy in an asymmetrical 2PIM drive dedicated to washing machine application. A special attention has been paid to the improvement of the drive energy efficiency. Such a target has been verified experimentally along with a high dynamic of the drive.

Referring to the previous literature review dealing with the control schemes dedicated to 2PIM drives, it has been noticed that the totality of the studied papers treated the implementation of indirect RFOC strategies in PWM-controlled B4- and B6-inverter fed 2PIM drives. This paper proposes the two direct RFOC schemes implemented in bang-bang (hysteresis)-controlled B4- and B6-inverter fed symmetrical 2PIM drives. This enables a rapid control of the power switches with the inverter commutation frequency kept constant by the sampling period of the digital signal processor in which the RFOC strategies are implemented. A comparison of the steady-state and transient performance of both drives, under the proposed RFOC strategies, is carried out for the sake of a firm selection of the inverter topology.

II. B4- and B6-Inverter Fed Two-Phase IM Drives

A symmetrical 2PIM is equipped with two identical phases, geometrically shifted by a 90° electrical angle, in the stator and a squirrel cage in the rotor. In order to develop an ideal circular rotating field, the stator phases should be fed by two sinusoidal currents shifted by 90°. Thanks to its reduced number of phases, the 2PIM represents a viable candidate for low-power low-cost applications. Moreover, it exhibits an improved compactness, which is of great interest for embedded actuators.

Further improvement of the cost effectiveness is gained with the reduction of the associated inverter topology which could be a B4 rather than a B6 in the case of 3PIMs. However, such a reduction could have some fallouts on the drive performance. These will be investigated following the implementation of two direct RFOC strategies in the B4- and B6-inverter fed 2PIM.

A. B4-Inverter Fed Two-Phase IM Drive

Fig. 1 shows the connections of a B4-inverter fed symmetrical 2PIM drive. The 2PIM phases, named "a" and "b," are series connected with their terminals linked to the B4-inverter legs, and with the neutral point "n" linked to the middle point "o" of the dc bus voltage $V_{\rm dc}$.

The states of the four power switches of the B4-inverter are denoted by the binary variables S_1–S_4. The stator phase-to-

TABLE I
SWITCH STATE COMBINATIONS, CORRESPONDING STATOR PHASE VOLTAGES, AND RESULTING ACTIVE VOLTAGE VECTORS $\mathbf{V_i}$ OF THE B4-INVERTER FED 2PIM IN THE CASE OF BALANCED DC-LINK CAPACITOR VOLTAGES $V_{\rm dc1} = V_{\rm dc2} = \frac{V_{\rm dc}}{2}$

$(S_1\,S_2)$	$v_{\rm an}$	$v_{\rm bn}$	$\mathbf{V_i}$
(1 1)	$\frac{V_{\rm dc}}{2}$	$\frac{V_{\rm dc}}{2}$	$\mathbf{V_1}$
(0 1)	$-\frac{V_{\rm dc}}{2}$	$\frac{V_{\rm dc}}{2}$	$\mathbf{V_2}$
(0 0)	$-\frac{V_{\rm dc}}{2}$	$-\frac{V_{\rm dc}}{2}$	$\mathbf{V_3}$
(1 0)	$\frac{V_{\rm dc}}{2}$	$-\frac{V_{\rm dc}}{2}$	$\mathbf{V_4}$

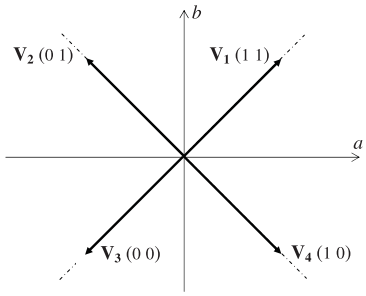

Fig. 2. Active voltage vectors $\mathbf{V_i}$ generated by a B4-inverter fed 2PIM.

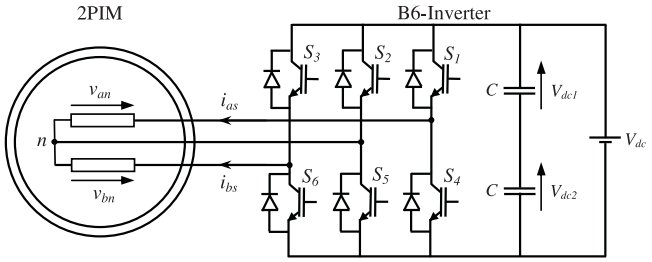

Fig. 3. B6-inverter fed 2PIM drive connections.

neutral voltages $v_{\rm an}$ and $v_{\rm bn}$ are expressed, in terms of the states S_1 and S_2 and the dc bus voltage $V_{\rm dc}$, as follows:

$$\begin{bmatrix} v_{\rm an} \\ v_{\rm bn} \end{bmatrix} = \begin{bmatrix} 1 & 0 & -\frac{1}{2} \\ 0 & 1 & -\frac{1}{2} \end{bmatrix} \begin{bmatrix} S_1 \\ S_2 \\ 1 \end{bmatrix} V_{\rm dc}. \tag{1}$$

Four active voltage vectors ($\mathbf{V_1}$–$\mathbf{V_4}$), corresponding to the combinations of the states S_1 and S_2, are defined in Table I.

These vectors are located, in the stationary a–b plane, as shown in Fig. 2. They have an amplitude equal to $\frac{V_{\rm dc}}{\sqrt{2}}$ and are shifted by 90°.

B. B6-Inverter Fed Two-Phase IM Drive

The B6-inverter fed 2PIM drive connections are shown in Fig. 3. Two among the three inverter legs are connected to the terminals of the 2PIM a- and b-phases; the third one is linked to the neutral point n.

The states of the six power switches of the B6-inverter are indicated by six binary variables S_1–S_6. The stator phase-to-neutral voltages $v_{\rm an}$ and $v_{\rm bn}$ are expressed, in terms of the states (S_1, S_2, and S_3) and the dc bus voltage $V_{\rm dc}$, as following:

TABLE II
SWITCH STATE COMBINATIONS, CORRESPONDING STATOR PHASE VOLTAGES, AND RESULTING VOLTAGE VECTORS $\mathbf{V_i}$ OF THE B6-INVERTER FED 2PIM

$(S_1\,S_2\,S_3)$	$v_{\rm an}$	$v_{\rm bn}$	$\mathbf{V_i}$
(0 0 0)	0	0	$\mathbf{V_0}$
(1 0 0)	$V_{\rm dc}$	0	$\mathbf{V_1}$
(1 0 1)	$V_{\rm dc}$	$V_{\rm dc}$	$\mathbf{V_2}$
(0 0 1)	0	$V_{\rm dc}$	$\mathbf{V_3}$
(0 1 1)	$-V_{\rm dc}$	0	$\mathbf{V_4}$
(0 1 0)	$-V_{\rm dc}$	$-V_{\rm dc}$	$\mathbf{V_5}$
(1 1 0)	0	$-V_{\rm dc}$	$\mathbf{V_6}$
(1 1 1)	0	0	$\mathbf{V_7}$

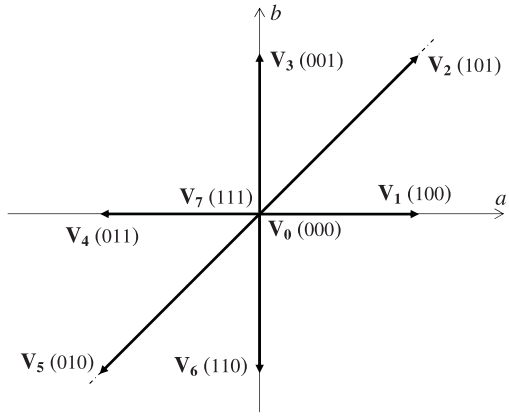

Fig. 4. Voltage vectors $\mathbf{V_i}$ generated by a B6-inverter fed 2PIM.

$$\begin{bmatrix} v_{\rm an} \\ v_{\rm bn} \end{bmatrix} = \begin{bmatrix} 1 & -1 & 0 \\ 0 & -1 & 1 \end{bmatrix} \begin{bmatrix} S_1 \\ S_2 \\ S_3 \end{bmatrix} V_{\rm dc}. \tag{2}$$

Table II gives the eight state combinations, the corresponding stator phase voltages, and the resulting voltage vectors $\mathbf{V_i}$. These could be classified as follows according to their amplitudes:

1) $\mathbf{V_1}$, $\mathbf{V_3}$, $\mathbf{V_4}$, and $\mathbf{V_6}$ are equal to $V_{\rm dc}$;
2) $\mathbf{V_2}$ and $\mathbf{V_5}$ are equal to $\sqrt{2}V_{\rm dc}$;
3) $\mathbf{V_0}$ and $\mathbf{V_7}$ are null vectors.

Vectors $\mathbf{V_i}$ are located in the a–b plane as shown in Fig. 4.

III. RFOC STRATEGY FORMULATION

The principle of the RFOC strategies dedicated to 2PIM drives is similar to the one introduced so far for the 3PIM drives [12]. The only difference is related to the variable changes from the stationary a–b frame to the one linked to the rotating field, also called synchronous d–q frame.

Let us consider the coordinate transform that enables the expression of the 2PIM variables defined in the stationary a–b frame in terms of those defined in the synchronous d–q one, as

$$\begin{bmatrix} x_a \\ x_b \end{bmatrix} = \begin{bmatrix} \cos\theta_e & -\sin\theta_e \\ \sin\theta_e & \cos\theta_e \end{bmatrix} \begin{bmatrix} x_d \\ x_q \end{bmatrix} \tag{3}$$

where θ_e is the position of the d-axis with respect to: 1) the stator a-phase axis for the stator variables; and 2) the rotor a-phase axis for the rotor ones.

TABLE III
SYMMETRIC 2PIM PARAMETERS

$r_s = 1.47\ \Omega$	$L_s = 13.6$ mH	$M = 11.7$ mH	$J = 2\text{e}^{-4}$ kg · m^2
$r_r = 0.39\ \Omega$	$L_r = 13.6$ mH	$N_p = 2$	$f = 2\text{e}^{-4}$ N · m·s

The ab-to-dq transform matrix is expressed as follows:

$$\begin{bmatrix} x_d \\ x_q \end{bmatrix} = \begin{bmatrix} \cos\theta_e & \sin\theta_e \\ -\sin\theta_e & \cos\theta_e \end{bmatrix} \begin{bmatrix} x_a \\ x_b \end{bmatrix}. \tag{4}$$

In order to achieve decoupled controls of the rotor flux and the electromagnetic torque, the rotor flux vector $\mathbf{\Phi_r}$ should be aligned along the d-axis, yielding $\phi_{\rm dr} = \phi_r$ and $\phi_{\rm qr} = 0$. Doing so, the dynamic model of the 2PIM, in such a d–q reference frame, is expressed as follows:

$$\begin{cases} v_{\rm ds} = r_s i_{\rm ds} + \dfrac{d}{dt}\phi_{\rm ds} - \omega_e \phi_{\rm qs} & (a) \\ v_{\rm qs} = r_s i_{\rm qs} + \dfrac{d}{dt}\phi_{\rm qs} + \omega_e \phi_{\rm ds} & (b) \\ 0 = r_r i_{\rm dr} + \dfrac{d}{dt}\phi_r & (c) \\ 0 = r_r i_{\rm qr} + \omega_{\rm sl}\phi_r & (d) \end{cases} \tag{5}$$

and

$$\begin{cases} \phi_{\rm ds} = L_s i_{\rm ds} + M i_{\rm dr} & (a) \\ \phi_{\rm qs} = L_s i_{\rm qs} + M i_{\rm qr} & (b) \\ \phi_r = M i_{\rm ds} + L_r i_{\rm dr} & (c) \\ 0 = M i_{\rm qs} + L_r i_{\rm qr} & (d) \end{cases} \tag{6}$$

where ($v_{\rm ds}$, $v_{\rm qs}$), ($i_{\rm ds}$, $i_{\rm qs}$), and ($\phi_{\rm ds}$, $\phi_{\rm qs}$) denote the stator voltages, currents, and flux, respectively; ($i_{\rm dr}$, $i_{\rm qr}$) and $\phi_{\rm dr}$ are the rotor currents and flux, respectively. (r_s, r_r) and (L_s, L_r) denote the stator and rotor resistances and self-inductances, respectively. M and $\omega_{\rm sl}$ are the mutual inductance and the slip angular frequency, respectively.

Accounting for (5c), (5d), (6c), and (6d), ϕ_r and $\omega_{\rm sl}$ could be expressed as follows:

$$\begin{cases} \phi_r = \dfrac{M}{1 + T_r p} i_{\rm ds} & (a) \\ \omega_{\rm sl} = \dfrac{M}{T_r}\dfrac{i_{\rm qs}}{\phi_r} & (b) \end{cases} \tag{7}$$

where $T_r = L_r / r_r$, and p is the differential operator.

The expression of the torque is then reduced to

$$T_{\rm em} = N_P \frac{M}{L_r} \phi_r i_{\rm qs} \tag{8}$$

where N_p denotes the pole pairs.

IV. RFOC IMPLEMENTATION IN CURRENT-REGULATED B4- AND B6-INVERTER FED 2PIM DRIVES

A. Case of B4-Inverter

The implementation of the direct RFOC strategy in a current-regulated B4-inverter fed 2PIM drive has the scheme shown in Fig. 5. The rotor flux, the slip angular frequency, and the electromagnetic torque are estimated using (7a), (7b), and (8), respectively. The speed, the torque, and the flux controllers are of PI-type. The dq-to-ab and ab-to-dq variable changes are done using matrices (3) and (4), respectively. Two two-level hysteresis controllers drive the inverter switches.

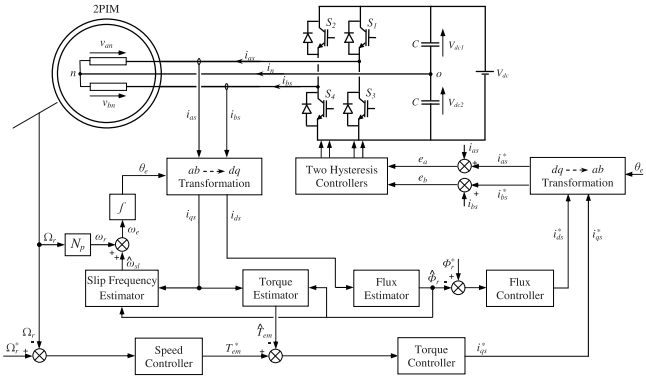

Fig. 5. Implementation scheme of the proposed direct RFOC strategy dedicated to a current-regulated B4-inverter fed 2PIM drive.

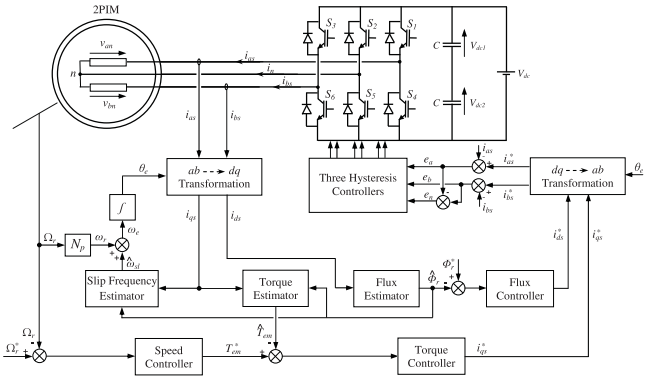

Fig. 6. Implementation scheme of the proposed direct RFOC strategy dedicated to a current-regulated B6-inverter fed 2PIM drive.

B. Case of B6-Inverter

The implementation of the direct RFOC strategy in a current-regulated B6-inverter fed 2PIM drive has the scheme shown in Fig. 6. It is similar to the one corresponding to the case of the B4-inverter illustrated in Fig. 5. The only difference lies in the control of the power switches which is achieved by two two-level hysteresis controllers in the B4-inverter rather than three in the B6-inverter, such that: 1) two hysteresis controllers drive the switches of the two legs connected to the stator phase terminals; and 2) the third one drives the switches of the inverter leg connected to the neutral point of the stator phases.

The input of the third hysteresis controller is the error e_n. It is equal to the difference between the desired neutral current i_n^* and the actual one i_n. It is easily predicted as

$$\begin{aligned} e_n &= i_n^* - i_n \\ &= -(i_{\rm as}^* + i_{\rm bs}^*) + (i_{\rm as} + i_{\rm bs}) \\ &= -(e_a + e_b). \end{aligned} \tag{9}$$

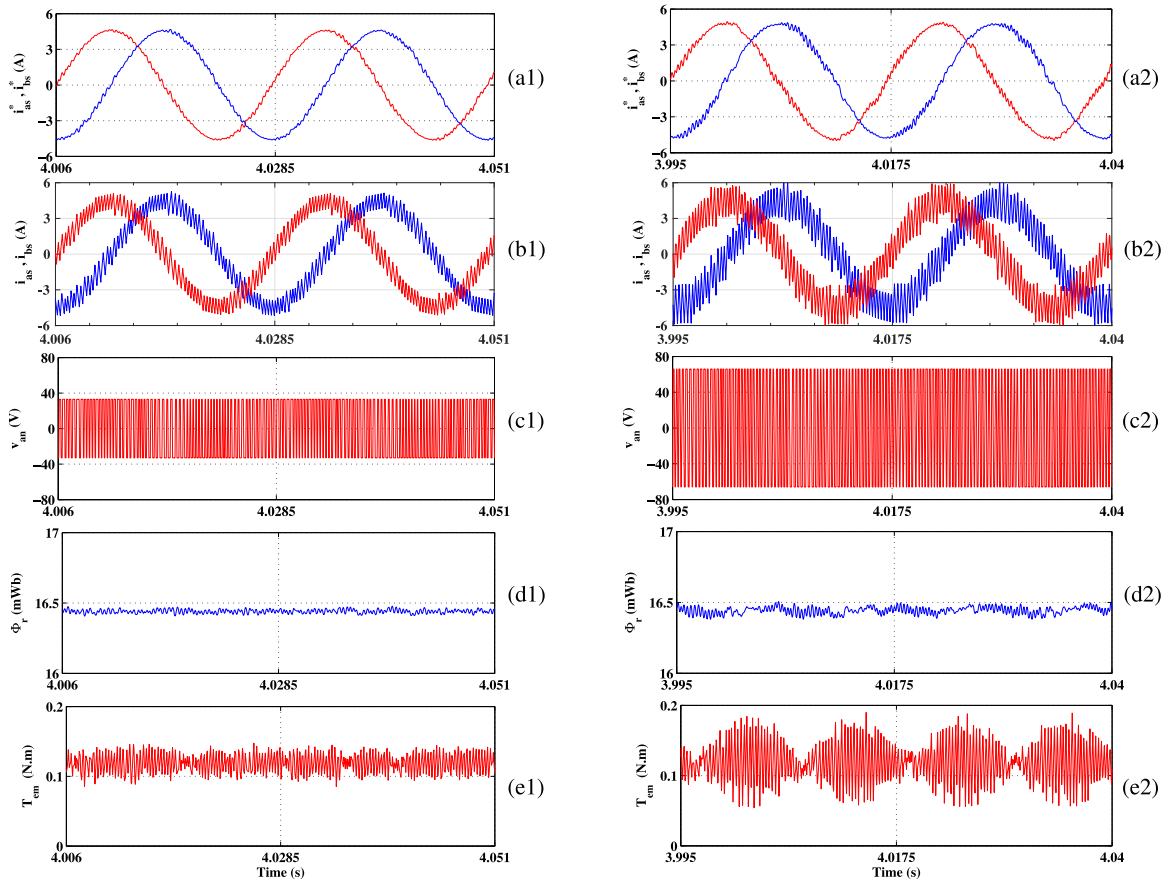

Fig. 7. Simulation results corresponding to the steady-state operation of the B4- (subscript "1") and the B6- (subscript "2") inverter fed 2PIM drives under the proposed direct RFOC strategies for $\Omega_r^* = 100$ rad/s. **Legend:** (a) $i_{\rm as}^*$ and $i_{\rm bs}^*$; (b) $i_{\rm as}$ and $i_{\rm bs}$; (c) $v_{\rm an}$; (d) ϕ_r; (e) $T_{\rm em}$.

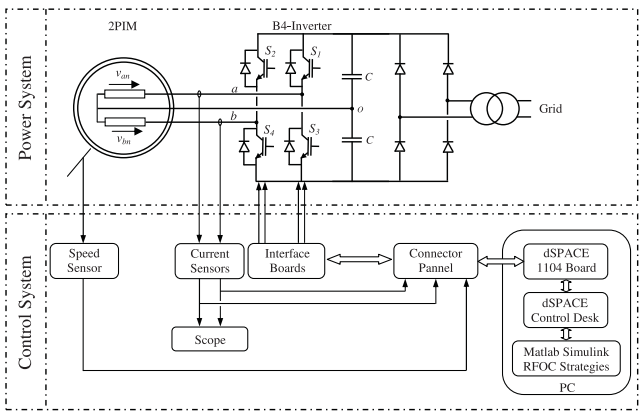

Fig. 8. Schematic block diagram of the developed test bench.

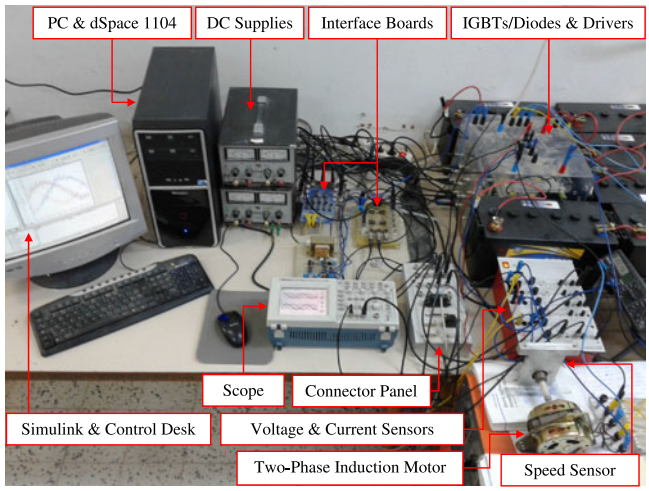

Fig. 9. Photograph of the experimental setup used for the implementation and performance investigation of the direct RFOC strategies.

V. Simulation-Based Investigation of Selected Steady-State Features of the 2PIM Drives Under Comparison

In this section, the performance of the direct RFOC strategies dedicated to both current-regulated B4- and B6-inverter fed 2PIM drives are predicted by simulation. These will be experimentally validated Section VI. The dc bus voltage $V_{\rm dc}$ is kept constant equal to 68 V. The sampling period T_s is equal to 50 μs. The parameters of the considered 2PIM are listed in Table III.

Fig. 7 shows the simulation results characterizing the steady-state operation of the 2PIM fed by the B4-inverter (subscript "1") and by the B6-inverter (subscript "2") under the control of the developed direct RFOC strategies, in the case of a reference speed $\Omega_r^* = 100$ rad/s. Subscripts (a)–(e) are assigned to the reference stator phase currents $i_{\rm as}^*$ and $i_{\rm bs}^*$, the actual stator

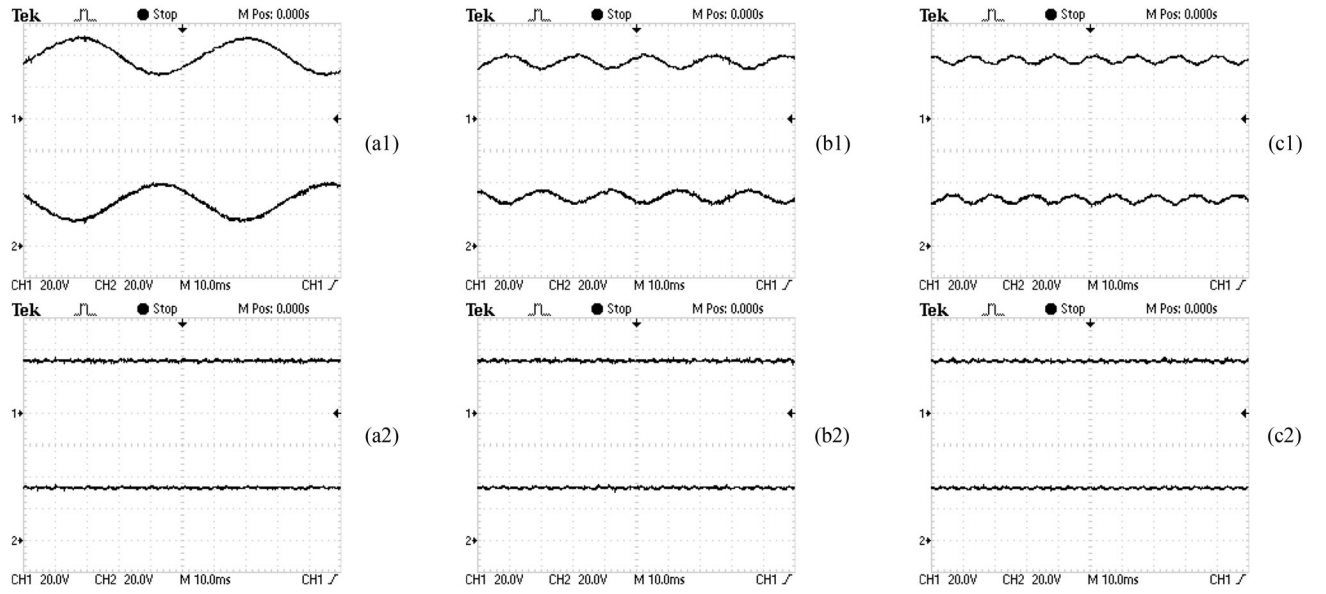

Fig. 10. Measured dc-link voltages at steady-state operation of the B4- (subscript "1") and the B6- (subscript "2") inverter fed 2PIM drives under the direct RFOC strategies. **Legend 1:** (top): $V_{\mathrm{dc}1}$, (bottom): $V_{\mathrm{dc}2}$ (20 V/div). **Legend 2:** (a) $\Omega_r^* = 10$ rad/s; (b) $\Omega_r^* = 100$ rad/s; (c) $\Omega_r^* = 200$ rad/s.

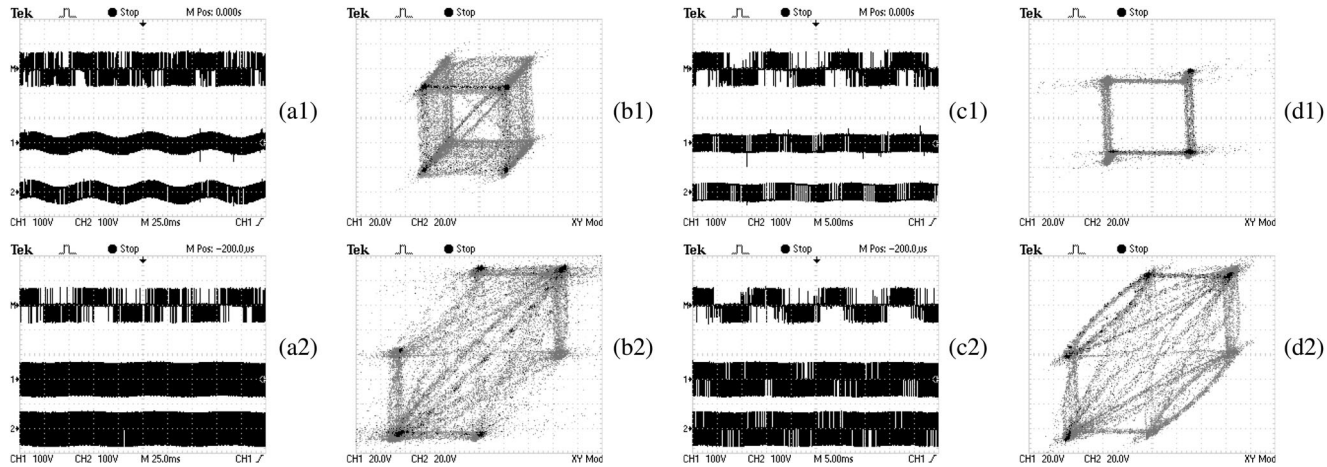

Fig. 11. Measured stator line-to-line and phase voltages at steady-state operation of the B4- (subscript "1") and the B6- (subscript "2") inverter fed 2PIM drives under the proposed direct RFOC strategies and for a loading level corresponding to the rated stator phase current $i_{s\,(\mathrm{rms})} = 3$ A. **Legend 1:** (a) and (c) (top): U_{ab}, (middle): v_{an}, (bottom): v_{bn} (100 V/div); (b) and (d) locus described, in the stationary a–b plane, by the extremities of the active voltage vectors (20 V/div). **Legend 2:** (a) and (b) $\Omega_r^* = 10$ rad/s; (c) and (d) $\Omega_r^* = 200$ rad/s.

phase currents i_{as} and i_{bs}, the stator a-phase voltage v_{an}, the predicted rotor flux ϕ_r in the synchronous reference frame, and the predicted electromagnetic torque T_{em}, respectively. Referring to Fig. 7(a) and (b), it is to be noted that the actual stator phase currents i_{as} and i_{bs} follow their references, and are shifted by $\frac{\pi}{2}$.

Moreover, the comparison between the results shown in Fig. 7(b1) and (b2) clearly highlights that the current ripple are higher in the case of the B6-inverter. As expected, these ripple have greatly affected the quality of the electromagnetic torque, as illustrated in Fig. 7(e2). It is to be noted that the current ripple are directly linked to the level of the stator phase voltages. These vary between $\pm V_{\mathrm{dc}}$ in the case of the B6-inverter and between $\pm\frac{V_{\mathrm{dc}}}{2}$ in the case of the B4-inverter, as shown in Fig. 7(c1) and (c2). From the analysis of Fig. 7(d1) and (d2), one can notice that the estimated rotor flux exhibits almost a ripple-free waveform in the case of the B4-inverter.

VI. Experiment-Based Investigation of the Steady-State and Transient Behaviors

The experiments have been carried out using a test bench built around a TMS320F240 DSP-based digital controller. Two electrolytic capacitors $2C$ are mounted in the input of the B4- and B6-inverters, with $C = 2200\ \mu$F. The inverter legs are made up of SKM 50 GB 123 D modules, which are associated SKHI 22 A drives to control the IGBTs. The dc bus voltage V_{dc}, the sampling period T_s, and the parameters of the 2PIM are the same as those considered in simulation.

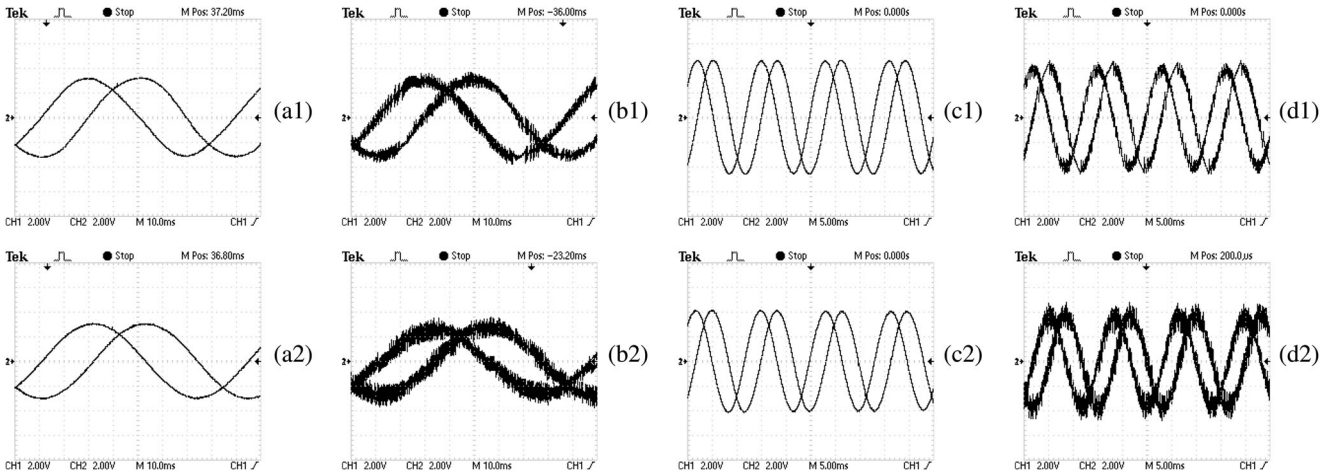

Fig. 12. Reference and measured stator phase currents at the steady-state operation of the B4- (subscript "1") and the B6- (subscript "2") inverter fed 2PIM drives under the proposed direct RFOC strategies. **Legend 1:** (a) and (c) $i_{\rm as}^{*}$ and $i_{\rm bs}^{*}$; (b) and (d) $i_{\rm as}$ and $i_{\rm bs}$ (2 A/div). **Legend 2:** (a) and (b) $\Omega_r^{*} = 10$ rad/s with $i_{s(\rm rms)} = 2.5$ A; (c) and (d) $\Omega_r^{*} = 200$ rad/s with $i_{s(\rm rms)} = 3$ A.

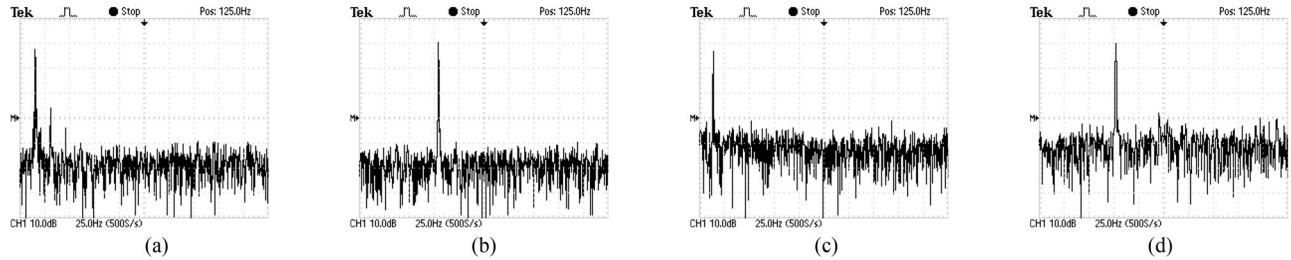

Fig. 13. (a)–(d) Spectra of the measured stator a-phase current shown in Fig. 12(b1), (d1), (b2), and (d2), respectively.

TABLE IV
SWITCH STATE COMBINATIONS, CORRESPONDING STATOR PHASE VOLTAGES, AND RESULTING ACTIVE VOLTAGE VECTORS $\mathbf{V_i}$ OF THE B4-INVERTER FED 2PIM IN THE CASE OF UNBALANCED DC-LINK VOLTAGES ($V_{\rm dc1} \neq V_{\rm dc2}$)

$(S_1\,S_2)$	$v_{\rm an}$	$v_{\rm bn}$	$\mathbf{V_i}$
(1 1)	$V_{\rm dc1}$	$V_{\rm dc1}$	$\mathbf{V_1}$
(0 1)	$-V_{\rm dc2}$	$V_{\rm dc1}$	$\mathbf{V_2}$
(0 0)	$-V_{\rm dc2}$	$-V_{\rm dc2}$	$\mathbf{V_3}$
(1 0)	$V_{\rm dc1}$	$-V_{\rm dc2}$	$\mathbf{V_4}$

The schematic block diagram of the test bench is illustrated in Fig. 8. A photograph of the experimental setup is shown in Fig. 9.

A. Steady-State Operation Analysis

1) DC-Link Capacitor Voltages: The measured dc-link capacitor voltages $V_{\rm dc1}$ and $V_{\rm dc2}$ are shown in Fig. 10, considering three values of the reference speed: (a) $\Omega_r^{*} = 10$ rad/s; (b) $\Omega_r^{*} = 100$ rad/s; (c) $\Omega_r^{*} = 200$ rad/s, with a motor constant loading level equal to 83% of its rated value (corresponding to an rms value of the stator phase current $i_{s(\rm rms)} = 2.5$ A).

Referring to Fig. 10(a1), (b1), and (c1), it clearly appears that the dc-link capacitor voltages are unbalanced in the case of the B4-inverter fed 2PIM drive, especially at low speeds. This limitation is due to uneven discharging of the dc-link capacitors leading to significant voltage ripple at low stator frequencies [13]–[15]. Furthermore, accounting for the connection of the neutral point of the 2PIM to the middle point of the dc bus, additional ripple due to the injection of harmonics caused by the d–q transformation are affecting the dc bus voltages. This statement will be confirmed by the spectral analysis of the stator phase current illustrated in Fig. 13. These perturbations affect the instantaneous values as well as the average ones of the dc bus voltages. For instance, in the case of $\Omega_r^{*} = 10$ rad/s, the average values of the upper and lower dc-link capacitor voltages are $V_{\rm dc1}^{(\rm av)} = 40$ V and $V_{\rm dc2}^{(\rm av)} = 28$ V, respectively.

The above described limitations are totally mitigated in the case of the B6-inverter for which the dc-link capacitor voltages are balanced, with ($V_{\rm dc1} = V_{\rm dc2} = \dfrac{V_{\rm dc}}{2} = 34$ V) in the whole speed range.

2) Stator Line-to-Line and Phase Voltages: Fig. 11 characterizes the steady-state operation corresponding to two operating points sharing the same loading level of the 2PIM (corresponding to the rated stator phase current $i_{s(\rm rms)} = 3$A) and differing by the speed, with: $\Omega_r^{*} = 10$ rad/s (subscripts "a" and "b"), and $\Omega_r^{*} = 200$ rad/s (subscripts "c" and "d").

Fig. 11(a1), (a2), (c1), and (c2) show the waveforms of the stator line-to-line and phase voltages. Fig. 11(b1), (b2), (d1), and (d2) illustrate the variations of the stator b-phase voltage $v_{\rm bn}$ with respect to the stator a-phase voltage $v_{\rm an}$ during 1 s. The resulting waveforms correspond to the locus described, in

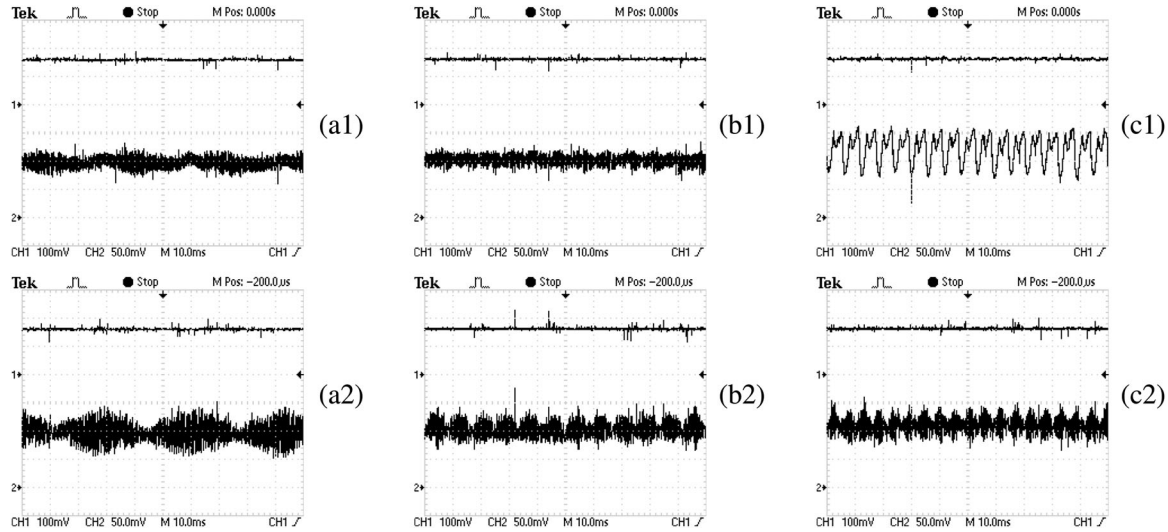

Fig. 14. Steady-state flux and torque of the B4- (subscript "1") and the B6- (subscript "2") inverter fed 2PIM drives under the proposed direct RFOC strategies for $i_{s\,(\mathrm{rms})} = 3$ A. **Legend 1:** (top) ϕ_r (10 mWb/div), (bottom): T_{em} (50 mN·m/div). **Legend 2:** (a) $\Omega_r^* = 10$ rad/s; (b) $\Omega_r^* = 150$ rad/s; (c) $\Omega_r^* = 250$ rad/s.

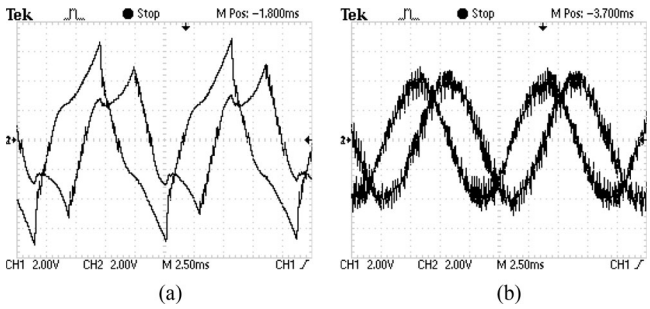

Fig. 15. Measured stator phase currents (2 A/div) at the steady-state operation of the 2PIM following the implementation of the proposed direct RFOC strategies for $\Omega_r^* = 250$ rad/s and $i_{s\,(\mathrm{rms})} = 3$ A. **Legend:** (a) case of the B4-inverter; (b) case of the B6-inverter.

the stationary a–b plane, by the extremities of the four active voltage vectors shown in Fig. 2 in the case of the B4-inverter and of the six active voltage vectors shown in Fig. 4 in the case of the B6-inverter.

From the analysis of Fig. 11(a1) and (c1), one can notice that the unbalanced dc-link voltages, penalizing the B4-inverter fed 2PIM drive, affect the stator phase voltages, especially at low speeds. The waveforms of the stator line-to-line and phase voltages exhibit a better regularity in the case of the B6-inverter.

Now, let us consider the locus described, in the stationary a–b frame, by the extremities of the four active voltage vectors generated by the B4-inverter shown in Fig. 11(b1) and (d1). If the dc-link capacitor voltages would have been balanced, such a locus would have a square shape with it summits correspond to the extremity of vectors $\mathbf{V_i}$ shown in Fig. 2 including both diagonals.

This is not the case of Fig. 11(b1) which shows a cubic shape due to the high unbalance of the dc-link capacitor voltages. Indeed, referring to Fig. 10(a1), one can notice the following: 28 V$\leq V_{\mathrm{dc1}} \leq$52 V and 16 V$\leq V_{\mathrm{dc2}} \leq$40 V. In the case of asymmetrical dc-link voltages ($V_{\mathrm{dc1}} \neq V_{\mathrm{dc2}}$), Table I turns to be Table IV.

Accounting for Table IV and for the above ranges of variation of V_{dc1} and V_{dc2}, one can find out an interpretation of the cubic shape of the locus described by the extremities of vectors $\mathbf{V_i}$.

This latter has a quasi-square shape at high speeds, as illustrated in Fig. 11(d1). This is due to the reduction of the asymmetry between the dc-link voltages, as shown in Fig. 10(c1). However, in the case of the B6-inverter, and referring to Fig. 11(b2) and (d2), one can notice almost the same shape which clearly highlights the summits of the voltage vectors $\mathbf{V_i}$ shown in Fig. 4.

3) Stator Phase Currents: Fig. 12 illustrates the waveforms of the reference (subscripts "a" and "c") and measured (subscripts "b" and "d") stator phase currents, considering two operating points characterized by: 1) $\Omega_r^* = 10$ rad/s with $i_{s\,(\mathrm{rms})} =$ 2.5 A (subscripts "a" and "b"); and 2) $\Omega_r^* = 200$ rad/s with $i_{s\,(\mathrm{rms})} = 3$ A (subscripts "c" and "d").

For both drives and for the two operating points, it is to be noted that the waveforms of the a- and b-phase reference and measured currents are balanced and shifted by $\frac{\pi}{2}$. Moreover, it is clearly appears that the phase current ripple are higher in the case of the B6-inverter. However, one can remark that the amplitude and the frequency of the reference currents are slightly higher in the case of the B4-inverter. This is explained by the fact that, for the same loading level, the 2PIM fed by the B6-inverter absorbs low current given its higher phase voltages. This remark is confirmed by the spectra shown in Fig. 13. These correspond (from left to right) to the harmonic contents of the measured a-phase stator currents i_{as}, shown in Fig. 12(b1), (d1), (b2), and (d2), respectively.

Furthermore, the spectra of Fig. 13 confirm the existence of the low-order harmonics in the case of the B4-inverter fed 2PIM. These are caused by the unbalanced dc bus voltages and the d–q transformation, especially at low stator frequencies. Both phenomena are eradicated in the case of the B6-inverter fed 2PIM.

4) Rotor Flux and Electromagnetic Torque: Fig. 14 gives the waveforms of the rotor flux ϕ_r and the electromagnetic torque T_{em} which have been estimated using the measured stator

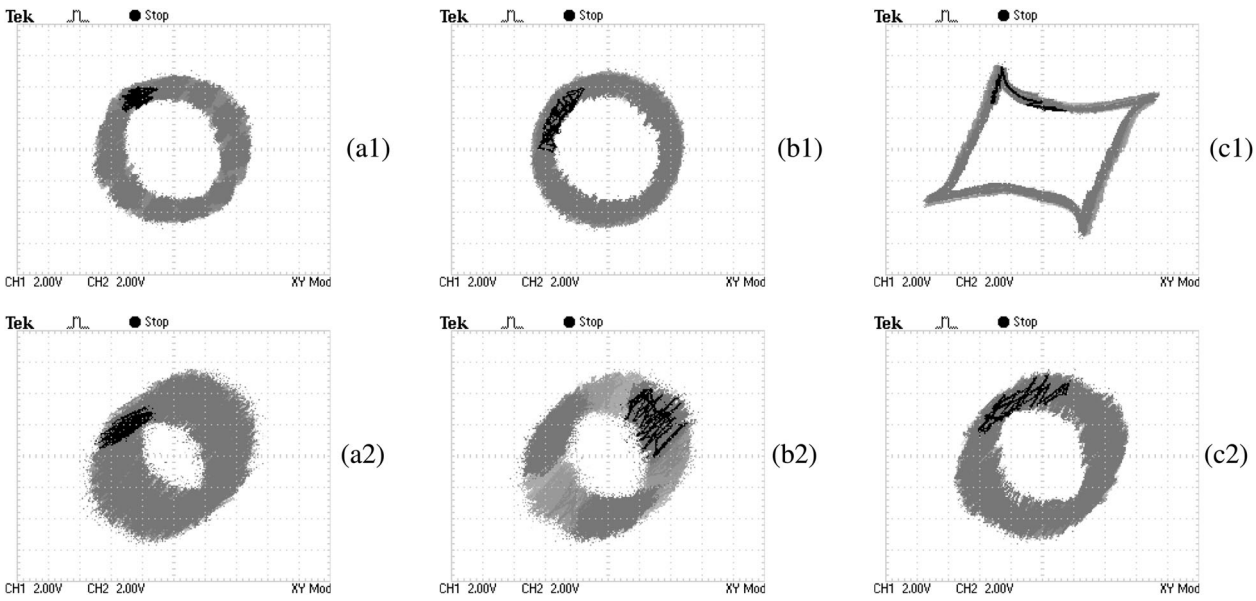

Fig. 16. Locus described by the extremity of $\mathbf{I_s}$ at the steady-state operation of the B4- (subscript "1") and the B6- (subscript "2") inverter fed 2PIM drives under the proposed direct RFOC strategies for $i_{s\,(\mathrm{rms})} = 3$ A. **Legend:** same as Legend 2 of Fig. 14.

phase currents for the same loading level, corresponding to the rated stator phase current $i_{s(\mathrm{rms})} = 3$ A, and for three reference speeds, such that: (a) $\Omega_r^* = 10$ rad/s; (b) $\Omega_r^* = 150$ rad/s; and (c) $\Omega_r^* = 250$ rad/s.

Referring to Fig. 14, it is to be noted that the rotor flux is constant and follows its reference $\phi_r^* = 16.6$ mWb for both drives. Moreover, as highlighted by the simulation results, the electromagnetic torque developed under the two first values of the reference speed has lower ripple in the case of the B4-inverter. However, from the comparison of Fig. 14(c1) and (c2), it clearly appears that for high speeds, the torque generated by the B4-inverter is affected by ripple indicating the initiation of an unstable operation. This is due to the fact that the capability of the B4-inverter to feed the 2PIM by the power required at high speeds is limited by the reduced phase voltage level. The B4-inverter commutations are then characterized by a four-step operation mode. Consequently, the generated phase currents turn to be distorted and unbalanced as shown in Fig. 15(a).

Fig. 16 shows the variations of i_{bs} with respect to i_{as}, considering the same operating points treated in Fig. 14. Ideally, the curves drawn in Fig. 16 should have a pure circular shape in so far as they represent the locus described by the extremities of the stator current vector $\mathbf{I_s}$ in the stationary a–b frame, which is not validated by experiments. Indeed, one can notice that the ripple of the stator phase currents are higher in the case of the B6-inverter, for low- and mid-speed ranges. However, at high speeds, the locus described by the extremity of $\mathbf{I_s}$, illustrated in Fig. 16(c1), is far from being circular. This is due to the distortion and unbalance of the amplitudes of i_{as} and i_{bs} in the case of the B4-inverter fed 2PIM drive, as confirmed by Fig. 15(a).

5) Summary: From the analysis of the previous steady-state experimental results, one can remark the following.

1) The implementation of the two direct RFOC schemes on bang-bang current-regulated B4- and B6-inverter fed 2PIM drives leads to decoupled controls of the rotor flux and of the electromagnetic torque. This clearly confirm that the bang-bang regulation of the phase currents is sufficiently rapid to control, with a high dynamic, the low-inertia 2PIM.
2) The phase currents as well as the electromagnetic torque exhibit lower ripple in the case of the B4-inverter fed 2PIM drive under the corresponding RFOC scheme. This has been gained thanks to the lower amplitude of the applied active voltage vectors, although the two dc bus voltages are affected at low speeds, by an asymmetry caused by an unequal discharge of the dc-link capacitors and an injection of harmonics due to the d–q transformation. These cause irregular amplitudes of the stator voltages.
3) The speed range is wider in the case of the B6-inverter fed 2PIM drive under the corresponding RFOC scheme. This has been gained thanks to the higher amplitude of the applied active voltage vectors.

In light of this analysis, it clearly appears that, beyond its improved cost effectiveness, the B4-inverter fed 2PIM drive exhibits higher performance under RFOC than the B6-inverter fed 2PIM one, except for its relatively limited speed range.

B. Transient Behaviors

1) Step-Shaped Reversal of the Reference Speed: Fig. 17 shows the experimental results giving the motor speed Ω_r, the electromagnetic torque T_{em}, and the rotor flux ϕ_r following three successive step-shaped reversals of the reference speed, such that $\Omega_r^* = \pm 100$ rad/s.

The comparison between the waveforms shown in Fig. 17(a1) and (a2) clearly highlights that the speed dynamic is faster in the case of the B6-inverter fed 2PIM drive. The B4-inverter fed 2PIM drive dynamic is remarkably affected by a zero-crossing distortion during the speed reversals characterized by a null step. Such a distortion is due to a torque cancellation period, as

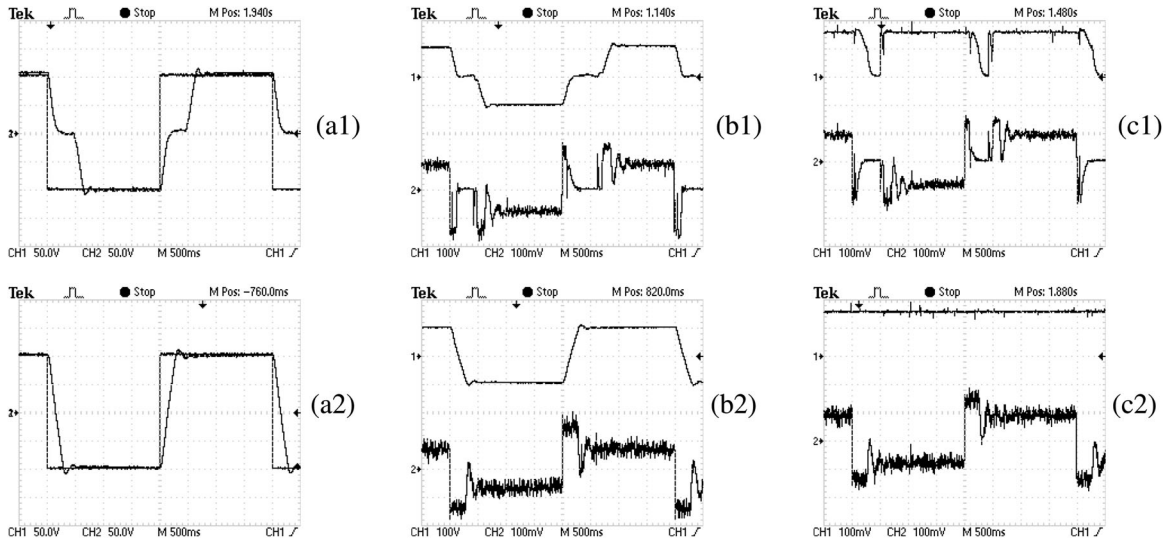

Fig. 17. Experimental investigation of the transient behaviors of the B4- (subscript "1") and the B6-(subscript "2") inverter fed 2PIM drives under the proposed direct RFOC strategies during three successive step-shaped reversals of the reference speed, with $\Omega_r^* = \pm 100$ rad/s. **Legend:** (a) Ω_r^* and Ω_r; (b) Ω_r and $T_{\rm em}$; (c) ϕ_r and $T_{\rm em}$.

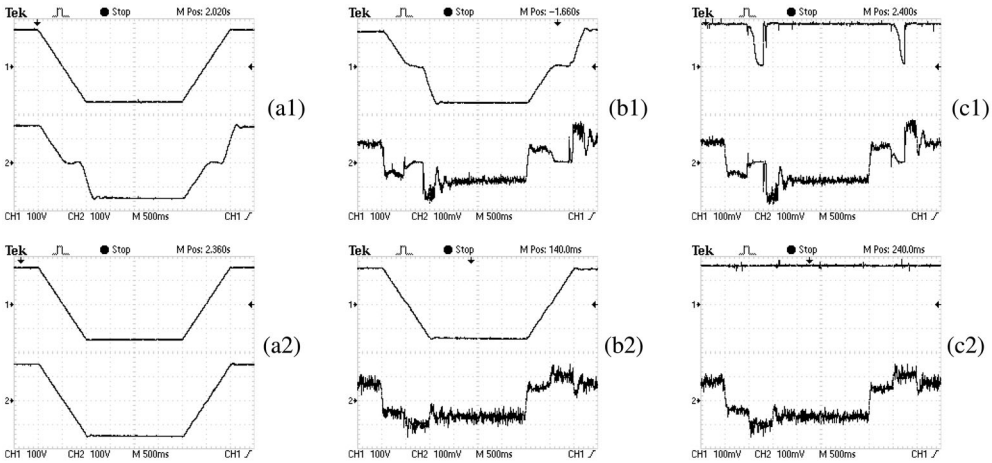

Fig. 18. Experimental investigation of the transient behaviors of the B4- (subscript "1") and the B6-(subscript "2") inverter fed 2PIM drives under the proposed direct RFOC strategies during two successive ramp-shaped reversals of the reference speed, with $\Omega_r^* = \pm 150$ rad/s. **Legend:** (a) Ω_r^* and Ω_r; (b) Ω_r and $T_{\rm em}$; (c) ϕ_r and $T_{\rm em}$.

shown in Fig. 17(b1), during which the 2PIM is no longer fed. This statement is confirmed by the annulment of the rotor flux as illustrated in 17(c1). These limitations are not applicable in the case of the B6-inverter fed 2PIM drive.

2) Ramp-Shaped Reversal of the Reference Speed: Fig. 18 shows the experimental results illustrating the motor speed Ω_r, the electromagnetic torque $T_{\rm em}$, and the rotor flux ϕ_r following two successive ramp-shaped reversals of the reference speed, such that $\Omega_r^* = \pm 150$ rad/s.

From the analysis of the waveforms shown in Fig. 18(a1), (b1), and (c1), it clearly appears that the phenomenon of the zero-crossing distortion penalizing the B4-inverter fed 2PIM drive perseveres even under a ramp-shaped speed reversals. In the manner of the step-shaped speed reversal, such a distortion is caused by the cancellation of the torque. However, the speed follows precisely its reference in the case of the B6-inverter fed 2PIM drive. These performance are gained thanks to the high dynamic of the torque and the accurate regulation of the rotor flux.

To sum up, the B4-inverter fed 2PIM drive suffers from a poor dynamic behavior during the speed reversals either they are step- or ramp-shaped. However, the B6-inverter fed 2PIM drive exhibits a high dynamic under both shapes of speed reversal.

VII. Conclusion

This paper was aimed at a comparison of the steady-state and transient performance of B4- and B6-inverter fed symmetrical 2PIM drives under dedicated RFOC strategies. The study has been initiated by a presentation of both drives and a briefly recall of the RFOC basis. Then, a special attention has been paid to the implementation of the direct RFOC on current-regulated inverters where the control of the power switches is achieved by two two-level hysteresis regulators in the B4-inverter rather than three in the B6-inverter.

A simulation-based comparison of selected steady-state features of both 2PIM drives under direct RFOC strategies has been carried out in a first step. Then, the comparison has been extended to a deep experimental investigation of the steady-state operation with emphasis on the dc-link capacitor voltages, the stator line-to-line and phase voltages, the stator currents, the rotor flux, and the electromagnetic torque. It has been found that the B4-inverter fed 2PIM drive suffers from the following three major limitations:

1) unbalanced dc-link capacitor voltages at low speeds;
2) a reduced speed range due to the low level of the phase voltages; and
3) an injection of harmonics due to the d–q transformation.

Moreover, the obtained results highlighted that the B6-inverter exhibits balanced dc-link capacitor voltages in the total constant torque region. However, it is penalized by higher phase currents and torque ripple.

The experiment-based comparison has been achieved by an investigation of the dynamic behaviors of both drives under step- and ramp-shaped reversals of the reference speed. It clearly revealed the superiority of the B6-inverter fed 2PIM drive compared to the B4 one. Indeed, this latter suffers from a zero-crossing distortion under both shapes of speed reversal.

To sum up, it has been clearly shown that, in spite of its higher cost, the B6-inverter is more suitable to feed symmetrical 2PIMs in order to achieve high performance in a large speed range. Consequently, a firm selection among the B4- and the B6-inverters should be based on the tradeoff cost/performance.

REFERENCES

[1] D. H. Jang, "PWM methods for two-phase inverters," *IEEE Ind. Appl. Mag.*, vol. 13, no. 2, pp. 50–61, Mar./Apr. 2007.

[2] S. Ziaeinejad, Y. Sangsefidi, H. P. Nabi, and A. Shoulaie, "Direct torque control of two-phase induction and synchronous motors," *IEEE Trans. Power Electron.*, vol. 28, no. 8, pp. 4041–4050, Aug. 2013.

[3] A. Ouarda, B. El Badsi, and A. Masmoudi, "DTC of B4 inverter fed two-phase IM drives," in *Proc. 13th IEEE Veh. Power Propulsion Conf.*, Hangzhou, China, Oct. 2016, pp. 1–6.

[4] R. P. Vieira, C. C. Gastaldini, R. Z. Azzolin, H. Pinheiro, and H. A. Grundling, "Simple PWM approach for modulation of three-leg inverters driving two-phase symmetrical and asymmetrical machines," in *Proc. 19th Int. Conf. Elect. Mach.*, Rome, Italy, Sep. 2010, pp. 1–6.

[5] Y. Kumsuwan, S. Premrudeepreechacharn, and V. Kinnares, "A carrier-based unbalanced PWM method for four-leg voltage source inverter fed unsymmetrical two-phase induction motor," *IEEE Trans. Ind. Electron.*, vol. 60, no. 5, pp. 2031–2041, May 2013.

[6] C. Charumit and V. Kinnares, "Discontinuous SVPWM techniques of three-leg VSI-fed balanced two-phase loads for reduced switching losses and current ripple," *IEEE Trans. Power Electron.*, vol. 30, no. 4, pp. 2191–2204, Apr. 2015.

[7] M. Jemli, H. Ben Azza, M. Boussak, and M. Gossa, "Sensorless indirect stator field orientation speed control for single-phase induction motor drive," *IEEE Trans. Power Electron.*, vol. 24, no. 6, pp. 1618–1627, Jun. 2009.

[8] M. Guerreiro, D. Foito, and A. Cordeir, "A speed controller for a two-winding induction motor based on diametrical inversion," *IEEE Trans. Ind. Electron.*, vol. 57, no. 1, pp. 449–456, Jan. 2010.

[9] S. Kascak, P. Zaskalicky, B. Dobrucky, and M. Prazenica, "Two-phase space vector modulation of FOC controlled ASM fed by 2-Phase VSI inverter," in *Proc. 15th Int. Power Electron. Motion Control Conf.*, Novi Sad, Serbia, Sep. 2012, pp. DS2c.13-1–DS2c.13-5.

[10] D. H. Jang, "Problems incurred in a vector-controlled single-phase induction motor, and a proposal for a vector-controlled two-phase induction motor as a replacement," *IEEE Trans. Power Electron.*, vol. 28, no. 1, pp. 526–536, Jan. 2013.

[11] A. Nied, J. de Oliveira, L. H. R. C. Stival, and H. B. Polli, "Improving washing machine performance using single-phase induction motor field-oriented control," in *Proc. 39th Annu. Conf. IEEE Ind. Electron. Soc.*, Vienna, Austria, Nov. 2013, pp. 2917–2922.

[12] F. Blaschke, "The principle of field orientation as applied to the new transvector closed-loop system for rotating-field machines," *Siemens Rev.*, vol. 34, no. 3, pp. 217–220, 1972.

[13] S. S. Wekhande, B. N. Chaudhari, S. V. Dhopte, and R. K. Sharma, "A low cost inverter drive for 2-phase induction motor," in *Proc. IEEE 1999 Int. Conf. Power Electron. Drive Syst.*, Hong Kong, China, Jul., 1999, pp. 428–431.

[14] M. A. Jabbar, A. M. Khambadkone, and Z. Yanfeng, "Space-vector modulation in a two-phase induction motor drive for constant-power operation," *IEEE Trans. Ind. Electron.*, vol. 51, no. 5, pp. 1081–1088, Oct. 2004.

[15] B. Kumar and S. Srinivas, "Space vector based PWM of dual full-bridge VSI fed two-phase induction motor drive," in *Proc. 23rd Int. Symp. Int. Electron.*, Istanbul, Turkey, Jun. 2014, pp. 667–672.

Ameni Ouarda received the B.S. and M.S. degrees, both in electrical engineering, from the Sfax Engineering National School, University of Sfax, Sfax, Tunisia, in 2011 and 2012, respectively. She is currently working toward the Ph.D. degree in electrical engineering from Sfax Engineering National School.

She is a member of the Research Laboratory on Renewable Energies and Electric Vehicles, University of Sfax. Her main research interests include the synthesis and the implementation of control strategies in induction motor drives applied to automotive actuators.

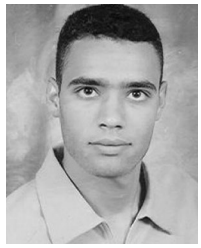

Bassem El Badsi received the B.S. degree in electromechanical engineering from the Sfax Engineering National School (SENS), University of Sfax, Sfax, Tunisia, in 2004, and the M.S., Ph.D., and Research Management Ability degrees, all in electrical engineering, from SENS, in 2005, 2009, and 2013, respectively.

In 2007, he joined the University of Gafsa as an Assistant Professor of power electronics and drives. In 2009, he joined SENS, University of Sfax, as an Associate Professor, where he has been a Professor since 2015. He is a member of the Research Laboratory on Renewable Energies and Electric Vehicles, University of Sfax. His research interests include power electronics and drives, and the implementation of advanced control strategies in ac motor drives applied to automotive systems.

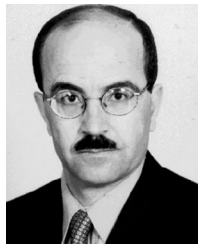

Ahmed Masmoudi (S'93–M'96–SM'99) received the B.S. degree from Sfax Engineering National School (SENS), University of Sfax, Sfax, Tunisia, in 1984, the Ph.D. degree from Pierre and Marie Curie University, Paris, France, in 1994, and the Research Management Ability degree from SENS, in 2001, all in electrical engineering.

In 1988, he joined the Tunisian University where he held different positions involved in both education and research activities. He is currently a Professor of electric power engineering with SENS. He is the Manager of the Research Laboratory on Renewable Energies and Electric Vehicles, University of Sfax. His main research interests include the design of new topologies of ac machines and the implementation of advanced and efficient control strategies in drives and generators, applied to automotive as well as in renewable energy systems.